Superelastic electron scattering by polarized excited sodium

T. Y. Jiang,[1,*] Z. Shi,[1] C. H. Ying,[1] L. Vušković,[2] and B. Bederson[1]
[1]*Physics Department, New York University, New York, New York 10003*
[2]*Physics Department, Old Dominion University, Norfolk, Virgina 23529*
(Received 4 November 1994)

Absolute differential cross sections for superelastic scattering have been measured for the sodium resonant transition in the incident electron energy range 3–20 eV. Results are obtained with no calibration being needed and are related to time-reversed inelastic scattering with unpolarized particles. Comparisons with distorted-wave, close-coupling, and convergent-close-coupling calculations are presented.

PACS number(s): 34.80.Dp

I. INTRODUCTION

The need to acquire experimental information concerning collisions of low-energy electrons with atoms that have been prepared in polarized excited states is well established by now. The low-energy range, defined here as being between 3 and 20 eV, is particularly interesting because it represents a regime where many aspects of the collision process, including target distortion, correlations, post-collision interaction, and exchange effects, play important, simultaneous roles, and, moreover, many collision channels (elastic, inelastic, and ionization) can be simultaneously open. While work on electron scattering by laser-excited atoms [1] is particularly scarce because of practical difficulties, such experiments are not only important because of their fundamental interest, but also in order to provide data relevant to more applied fields in which short-lived excited-state atomic collisions play a significant role. A detailed analysis of our current understanding of the process of collisional alignment and orientation of ground-state atoms by electron impact, which can be regarded as the time inverse of the process of electrons scattered by excited-state atoms, is presented in the review by Andersen, Gallagher, and Hertel [2].

The effective one-electron sodium atom has become a test case for electron-atom collision studies because of its experimental convenience and the relative simplicity it offers to theoretical models. For example, since sodium is a light alkali-metal atom, electron exchange plays an important role in electron-sodium scattering [3], but explicitly spin-dependent forces (spin-orbit interaction between projectile and target) may be neglected.

Traditional inelastic electron-sodium scattering experiments are performed employing ground-state sodium, for which the colliding electron transfers energy to the target atom. In the "time-inverse" reaction, scattering by excited $(3P)$Na results in a deexcitation of the atom and a corresponding increase in the kinetic energy of the colliding electron. To study such superelastic processes involving short-lived excited states, excited atoms must be continuously produced within the collision volume by laser excitation. As a consequence, the target atoms will possess uneven populations of $M_L = -1, 0, +1$ magnetic sublevels. Specifically, irradiation with circularly polarized laser light will result in the production of polarized, excited atomic targets [4]. In the present experiment the initial state of the target was *polarized* Na($3P$, $M_L = +1$) in the natural frame [2] (along the laser propagation axis, which is perpendicular to the scattering plane). Using a recoil-atom scattering method [5] we have obtained absolute superelastic differential cross sections for *unpolarized* Na($3P \rightarrow 3S$) as though the initial state of the target was prepared with an equal population of magnetic substates [6]. We present data in the low-energy range, as we have defined it, obtained with no calibration being needed. We have previously published preliminary results at 3 eV [7]. In the present case our results with unpolarized electrons and polarized $(3P)$Na atoms can be related [8] to the inelastic $3S \rightarrow 3P$ transition involving unpolarized electrons and atoms. Thus the recoil-atom scattering method provides an independent check of the traditional electron scattering experiment with unpolarized beams.

Superelastic and inelastic processes for $(3P)$Na were studied first using unpolarized incident electrons by Hertel and Stoll [9] and Hermann *et al.* [10], by measuring electron-scattering intensities as a function of the polarization of laser light, and thus determined the relative multipole moments T_0^2 and T_1^2. The spin polarization of superelastically scattered electrons, initially unpolarized, was measured by Hanne, Szmytkowski, and van der Wiel [11]. A series of experiments [4,12–16] has been performed at the National Institute of Standards and Technology (NIST) using a polarized incident electron beam to study superelastic electron scattering by $(3P)$Na prepared with linear or circular polarization of the laser light. In the NIST work spin dependence in superelastic collisions as a function of laser polarization as well as of electron energy was studied. The polarization of the scattered electrons in superelastic scattering by $(3P)$Na was measured by Teubner and Scholten [17].

This same electron-sodium–scattering problem has

*Present address: Arbin Corp., 623 San Mario, College Station, TX 77845.

also been the subject of intense theoretical interest over the past three decades. Results up to 1992 are summarized by Madison, Bartschat, and McEachran [18]. In the energy range of the present work the most successful calculations are performed using close coupling [19–21] (CC) based on the R-matrix approach [22], the convergent-close-coupling approach [23,24] (CCC), and the second-order Born distorted-wave [18,25] (DWB2) approximations. CC calculations [19] based on a semiempirical local representation for the atomic core potential acting upon the valence and scattering electrons have been improved with numerical methods [20,21] that treat differently low-, intermediate-, and high-order partial waves. The CCC method treats a "three-body" system and expands the total wave function in a large truncated Laguerre basis, enabling the application of standard close-coupling techniques to the resultant coupled equations. The "exact" nonrelativistic DWB2 calculations for sodium [18] incorporate the effects of the atomic charge cloud polarization, absorption, and electron exchange distortions into the calculation of the distorted waves. Here "exact" means that the infinite sums over the intermediate bound and continuum target states were performed without making approximations. These approximations are applicable in different parts of the energy region of the present work (or, the case of CCC, over the full region) and the results of our measurements can offer a test of the relative reliability of these several approximations in the overlapping range.

In the following sections an overview of the experimental method employed in the present research is described. This is followed by a presentation and an analysis of experimental results. Discussion of the results is presented in terms of time-reversed inelastic scattering with unpolarized particles and a comparison with CC, CCC, and DWB2 calculations is made.

II. EXPERIMENT

A. General setup

The apparatus used for the present experiments was constructed to measure cross sections for electron scattering by atoms using the atomic-recoil technique. This technique involves observation of the scattered atom beam after being cross fired by an electron beam, in the presence of a mutually perpendicular laser beam tuned to the sodium resonant $3\,^2S_{1/2}(F=2,\ M_F=2) \rightarrow 3\,^2P_{3/2}(F=3,\ M_F=3)$ transition. The production and detection of atom and electron beams and other experimental details are fully described in previous publications [5,26,27]. The photon beam and a quantitative analysis of the deflection of a sodium beam by laser radiation force in the traveling-beam arrangement (explained in Sec. II B) have been discussed in Ref. [28]. For convenience we recall briefly the essential parts of the experimental setup. Additional information and improvements in our data-taking protocols are also presented.

A schematic diagram of the experimental arrangement is shown in Fig. 1. The electron, the atom, and the laser beams intersect each other at right angles. Coordinate

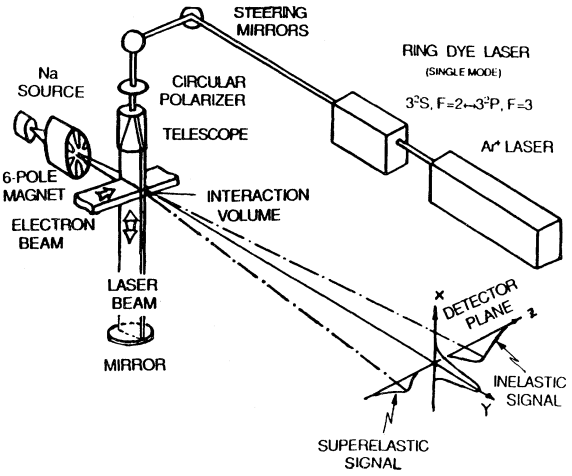

FIG. 1. Experimental arrangement. The electron, the atom, and the laser beams cross each other at right angles.

axes are such that the polar scattering angle θ lies in the scattering plane defined by the electron (z) and the atom (y) axes of propagation. Along the $+z$ axis $\theta=0°$. The projection of the azimuthal scattering angle ϕ is in the plane of the atom ($+y$) and the photon ($-x$) beams' propagation axes. Along the $+y$ axis $\phi=0°$.

The atomic-recoil type of experiment requires a well-collimated and velocity-selected atom beam as well as a large separation between the collision and the atom detection regions to achieve good angular resolution. The total length of the vacuum envelope is about 5 m, containing four mutually connected vacuum chambers. Each chamber can be moved on its own mounting platform for a coarse alignment of the entire apparatus. All internal components such as the atom-beam oven, the electron gun, and the detector, etc., are connected to external precision positioners through vacuum bellows so that fine alignment can be achieved by adjusting these positions carefully. The interaction and detection chambers are connected through a flexible bellows by a 3-m-long drift tube [26] that can rotate around the collision region. The detector chamber is also capable of independent vertical and horizontal translational motion [5]. A precision two-dimensional monitor records the detector position during runs. By this construction the detector can move over the surface of a sphere of radius $L=3.5$ m centered on the collision volume, thus enabling us to perform two-dimensional scans of the angular distribution of the atoms that have recoiled upon collisions with electrons.

A hexapole magnet [5,26] is located between the atom-beam source and interaction chambers, which serves to focus atoms on the atom-beam detector [26]; it also partially velocity and state selects the atom beam.

The construction [26] of the atom-beam source and its operational characteristics in the present experiment have been described previously [27]. The vapor pressure in the source of about 30 Torr was produced at a temperature of 880 K with a snout at 960 K. The atom beam passed through a 0.25-mm orifice drilled in the cap of the

snout. The spatial distribution of the beam was routinely measured in the detector plane. The atom-beam velocity distribution was determined using laser-induced fluorescence [27].

The construction of the electron gun [5,26] and the procedure to determine characteristics of the electron beam [27] have also been explained previously. Determinations of the nominal electron energy and the electron energy distribution are based on the measurements of Na^+ ions and a Wannier [29] threshold behavior of the total ionization cross section. The electron-beam number current in the present experiment was in the range of 10^{15} electrons/s.

Data-taking procedures and all geometrical parameters of the present experiment are given in Ref. [27]. However, for the present work an additional parameter is required, namely, the fraction of the excited atoms f, in the interaction volume, as explained in the following subsection. The laser system used in the present work has also been described [26,30] before.

B. Preparation of the initial atomic state

Two methods are used in our laboratory to prepare laser-excited $(3P)$Na atoms. If the laser beam passes through the interaction region in one direction only we call it a traveling-wave [28] laser-field configuration. This method of preparation, where the displacement of the photon-recoiled atom beam in the detector plane [30] is related to the excited-state fraction f of the atoms in the interaction region, has been used successfully in previous total [26,31,32] and elastic differential [30] cross-section measurements. A standing-wave [33] laser-field configuration is a second method of preparation that can be established by reflecting the laser beam back into the interaction volume.

We found that the traveling-wave laser-field configuration is not suitable for absolute measurements of the inelastic or superelastic differential cross sections in the atomic-recoil experiment. With the traveling-wave configuration the scattered atoms experience double recoil, i.e., recoil caused by both electrons and photons. In the present experiment, to prepare the initial state $(3P)$Na by laser excitation, ground-state $(3S)$Na atoms are originally prepared into $F=2$ states. In inelastic and superelastic $(3P)$Na processes, however, the atoms may decay to the nonresonant $F=1$ ground state due to electron excitation or deexcitation and become lost to the laser excitation process. For instance, for inelastic-scattering atoms are excited from $3\,^2P_{3/2}$ to $4S$, $3D$, etc., by electron impact after which they decay back to the $3\,^2S_{1/2}(F=1)$ or the $3\,^2S_{1/2}(F=2)$ state with roughly comparable probabilities. During the measurement the detector is set at the peak of the photon recoiled atomic beam in the $-x$ (laser axis) direction and scanned along the z (electron axis) direction. Therefore, the atoms that decay to the $(F=1)$ ground state no longer absorb photons, resulting in a partial loss of signal at the displaced detector.

Also, in our inelastic [7] and superelastic-scattering experiments, the measured scattering signals are attributable mainly to small-angle scattering. The spatial distribution of the recoiled atoms is influenced strongly by the atom-beam velocity distribution. Since in the traveling-wave laser-field configuration the deflected beam profile is modified by the atom-beam velocity distribution in the x direction, the slower atoms will be deflected further from their original position in the detector plane. This effect changes the atom-beam velocity distribution at each part of the beam profile and introduces an additional complication in the analysis of the experiment. Therefore, the spatial broadening of the deflected beam profile may cause larger errors in the measurement.

From the above discussion it is clear that an undeflected and narrowed atom beam is more suitable for the superelastic and the inelastic measurements and accordingly it is better to employ a standing-wave laser configuration field. In this case the radiation pressure due to the two counterpropagating waves can be added independently since at relatively low laser intensity [34] stimulated emission events are negligible. Thus the *average* momentum transfer from both laser directions will cancel out.

For circular polarized light produced by a Glan prism linear polarizer and a quartz zeroth-order quarter wave plate, the polarization direction of the reflected beam in the interaction volume is the same as that of the incident beam. After passing the interaction volume the reflected beam is restored to linearly polarized light by a quarter wave plate with the polarization direction perpendicular to that of the incident linearly polarized light. Therefore, it is reflected out of the axis of the incident laser beam by the linear polarizer, thereby avoiding feedback of light into the dye laser. There is no quarter wave plate if linearly polarized light is used. In this case the reflected beam may feed into the dye laser and cause the laser frequency to become unstable. Therefore, if a standing-wave laser field is employed, only circularly polarized light can be used.

In order to tune the laser frequency coarsely, laser-induced fluorescence in a sodium vapor cell is used. In the traveling-wave experiment a fine tuning is accomplished by monitoring the deflection of the atom beam, while, of course, in the standing-wave experiment there is no atom-beam deflection. Thus an absolute determination of the proper laser frequency needed to excite the atoms was achieved by measuring the Doppler-free saturated absorption spectrum [35] of the sodium D_2 line. The experimental setup is shown in Fig. 2. Two counterpropagating laser beams (probe and pump) overlap in a sodium vapor cell. The intensity of the probe beam is about 1% of the pump beam. The operation of such a device can be understood by hole burning in velocity space. Assuming that the laser frequency is shifted from the atomic resonance by a small amount, the two counterpropagating laser beams will be adsorbed by two different velocity groups of atoms because of the Doppler shift. When the laser frequency is on resonance, both probe and pump beams are absorbed by the same group of atoms with a zero-velocity component along the laser beam axis. In that case, when the absorption of these atoms has been nearly saturated by the pump beam, the

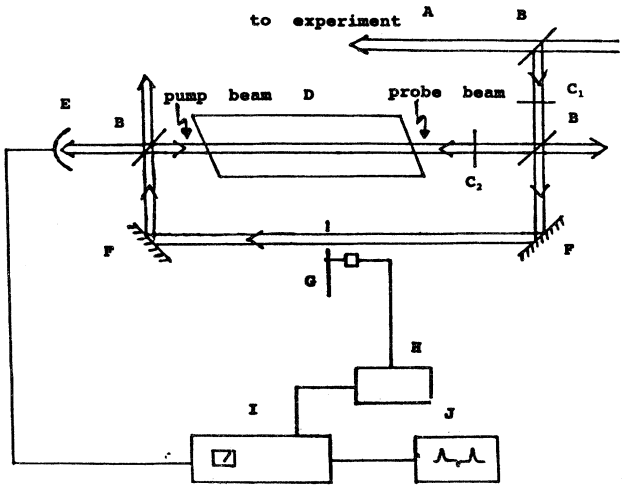

FIG. 2. Experimental arrangement for saturation spectroscopy: A, laser beam; B, beam splitters, 90% transparency; C_1, attenuator, 50% transparency; C_2, attenuator, 2% transparency; D, Na vapor cell; E, photodiode; F, mirrors; G, light beam chopper; H, chopper controller; I, lock-in amplifier; J, x-y plotter.

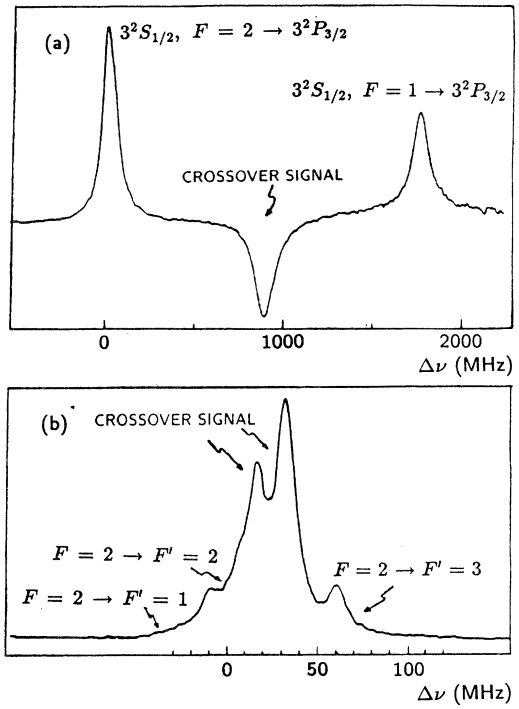

FIG. 3. Signals from saturation measurements. (a) $3\,^2S_{1/2} \rightarrow 3\,^2P_{3/2}$. (b) $3\,^2S_{1/2}(F=2) \rightarrow 3\,^2P_{3/2}(F=1,2,3)$. For simplicity, F indicates ground-state and F' excited-state levels.

probe beam will be absorbed less. In other words, the transmission of the probe beam is increased, resulting in an intensity peak in the spectrum at resonance when the laser frequency is scanned; to increase the contrast, the pump beam is chopped and the probe beam amplified using a lock-in detector. The spectrum of the $3\,^2S_{1/2} \rightarrow 3\,^2P_{3/2}$ transition is shown in Fig. 3(a). The negative peak between the two positive peaks is the crossover signal [36], which corresponds to the Doppler-shifted resonance involving a common excited state and both $3\,^2S_{1/2}(F=1,2)$ ground states. In this case the population of the state that resonates with the probe beam is increased by optical pumping of the pump beam resulting in a lowering of the transmission of the probe beam. Figure 3(b) shows the hyperfine structure of the $3\,^2P_{3/2}$ state obtained by reducing the scan width of the laser frequency. The arrows indicate the transitions $3\,^2S_{1/2}(F=2) \rightarrow 3\,^2P_{3/2}(F=1,2,3)$. For simplicity, in Fig. 3(b), F indicates ground-state and F' excited-state levels. Again, the crossover signals show up between these transitions, which correspond to the Doppler-shifted resonances involving a common ground state and two different excited states. The deeper saturation results in a higher transmission of the probe beam [36]. The Doppler-free resonance peak that corresponds to the transition $3\,^2S_{1/2}(F=2) \rightarrow 3\,^2P_{3/2}(F=3)$ is well separated from the others. It allows the absolute, precise determination of the laser frequency. To avoid collision broadening and power broadening in the sodium vapor cell, its temperature is kept at 100 °C and the laser power is kept at typically about 10^{-3} and 10^{-5} W for the pump and the probe beam, respectively. Higher cell temperature or higher laser power makes the peaks broaden and become indistinguishable.

In the standing-wave laser field the atom-beam spatial distribution is affected by the laser frequency. To understand qualitatively the influence, one can consider the standing-wave configuration as two counterpropagating traveling waves with the same frequency. The net radiation pressure is the superposition of those from both laser beams. When the laser frequency is red detuned, diverging atoms will be closer to resonance than converging ones causing a focusing effect. When the laser frequency is blue detuned, the atom beam will be defocused in the vertical direction. In Fig. 4 we show vertical atomic-beam profiles obtained with different laser frequencies. It can be seen that the beam profile obtained with small red detuning is the most suitable for a high-resolution atomic-beam experiment. On the other hand, small blue detuning is better to achieve a high fraction of excited atoms. A redshift of the laser frequency will increase the probability of exciting the $3\,^2P_{3/2}(F=2)$ state, which is only about 60 MHz below the desired $3\,^2P_{3/2}(F=3)$ state. Thus the fraction of atoms ending in the nonresonant $F=1$ ground state will increase. We performed an experiment to study this problem quantitatively. Laser-induced fluorescence is measured with a part of the laser beam, about 1 mW, transferred by a single-mode optical fiber to form a probe beam that crosses the atom beam perpendicularly 1 m downstream from the interaction region. By chopping the laser beam in the interaction region and comparing the fluorescence intensities in the probing region, the ratio of the number of atoms in the resonant ($F=2$) ground state with and without optical pumping can be obtained. Thus the fractions of the atoms that leak to the nonresonant ($F=1$) ground state

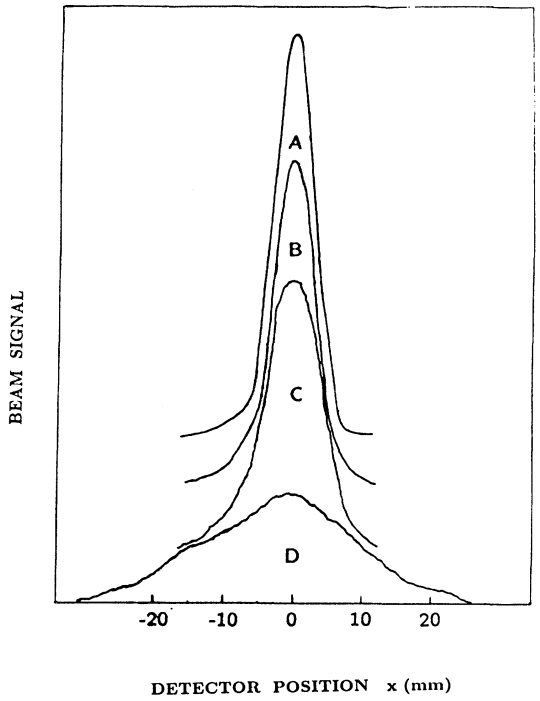

FIG. 4. Atom-beam vertical profiles obtained with different laser frequencies: *A*, laser-off FWHM of 5.5 mm; *B*, 8-MHz red detuning FWHM of 5.2 mm; *C*, on-resonance FWHM of 7.5 mm; *D*, 8-MHz blue detuning FWHM of 22 mm.

can be determined as a function of the laser frequency. These fractions of a full beam are 48% with 8-MHz red detuning, 35% with zero detuning, and 26% with 8-MHz blue detuning. Combining both considerations, the vertical atom-beam focusing and the fraction of excited atoms in the interaction region, we chose zero detuning in the experiment. Spatial distributions of atomic-beam profiles obtained with standing and traveling laser-beam conditions are shown in Fig. 5. In the standing-wave case the atom beam maintains practically the same full width at half maximum (FWHM) of both profiles. The small broadening is mainly due to photon statistics. Therefore, for this case the chance for the recoil atoms to enter the detector depends only on the electron-scattering process itself. Comparing these profiles with the traveling-wave case, the FWHM of the vertical one is narrower by a factor of 2. It can be seen from the equations in the following subsections that the width of the atom-beam vertical profile determines the azimuthal uncertainty of the final data. For example, with the present standing-wave conditions, for 10-eV electrons at $\theta=3°$ the atom-beam detector subtends azimuthal angles from $-15°$ to $+15°$.

An important part of the present experiment is the determination of the fraction of excited atoms in the interaction region. As mentioned above, in the traveling-wave laser-field configuration f is proportional [30] to the atom-beam displacement due to photon recoil. In the present experiment the laser-induced fluorescence intensities from traveling-wave and standing-wave fields are compared since in both cases fluorescence intensity is proportional to f. Thus the standing wave f is calibrated to the measured traveling wave f. We found f to be 0.26 with an incident laser intensity of 120 mW/cm^2. The uncertainty of 10% in f determination is attributable to the determination of the deflected peak position in the measurements of f in the traveling-wave configuration (6%) and relative fluorescence intensity in standing- versus traveling-wave configuration.

C. The recoil-atom method in superelastic scattering

Our recoil-atom analysis [5,27] is based on the approximation that the change of the longitudinal velocity in the

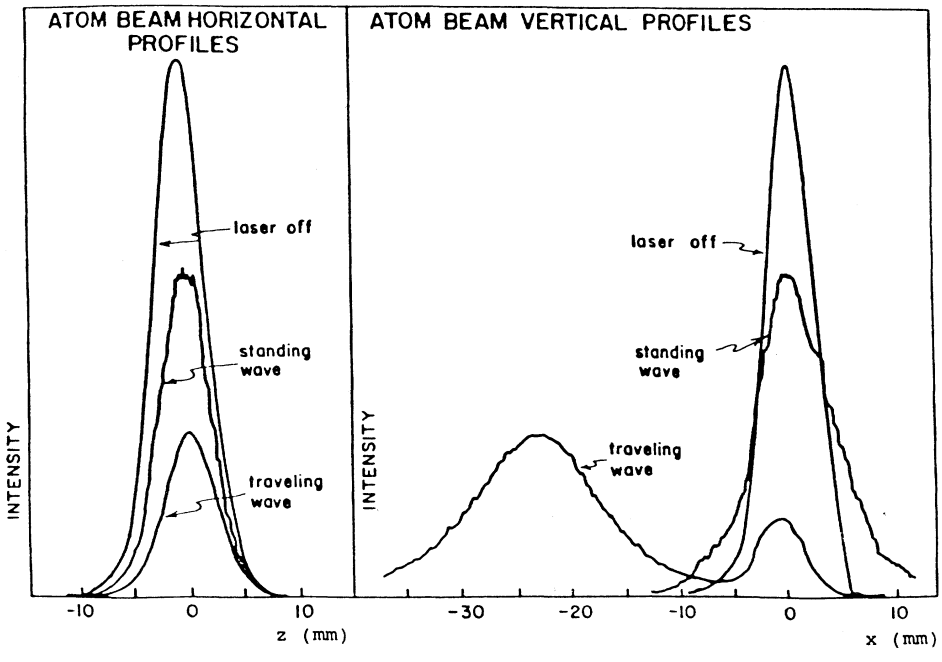

FIG. 5. Atom-beam profiles under the standing-wave and traveling-wave laser-field configurations.

collision is negligibly small as compared to the incident atomic velocity. This approximation is appropriate for the present experiment, where the atomic beam possesses a monochromaticity of 1200±200 m/s and the change of velocity in the collision is several m/s. Thus electrons scattered at both (θ,ϕ) and $(\theta,\pi-\phi)$ will cause the atoms to recoil into the same position in the detector plane. Therefore, for each θ both azimuthal angles (ϕ and π-ϕ) are recorded. In the present experiments the scattering signal is recorded in the scattering plane, so that ϕ is 0 or π.

The measured recoiled-atom intensity $I_s(z_D)$ of superelastic collisions at the detector position centered at z_D is related to the differential cross section $\sigma(\theta)$ and the relevant beam and apparatus parameters by the modified master equation [7]

$$I_s(z_D)=\frac{fi_0I_0(0)}{4h\Delta x\Delta z}\int_0^{\theta_{\max}}\sigma(\theta)\sin(\theta)d\theta\int_{E_0-\delta E}^{E_0+\delta E}\mathcal{E}(E)dE\int_{z_1}^{z_2}Z(z)dz\int_{V_1}^{V_2}\frac{\mathcal{V}(V)}{V}dV\int_{x_1}^{x_2}X(x)dx\int_{\phi_1}^{\phi_2}d\phi\ . \tag{1}$$

The parameters in Eq. (1) are the fraction of excited atoms f, the total electron number current i_0, the atom-beam current $I_0(0)$ at $z_D=0$, the height of the interaction region perpendicular to the scattering plane $h=0.8$ mm, the half-height $\Delta x=0.5$ mm and the half-width $\Delta z=0.5$ mm of the atom beam detector, the electron energy distribution $\mathcal{E}(E)$, the nominal electron energy E_0, the half-width of the electron energy distribution δE, the atom-beam velocity distribution $\mathcal{V}(V)$, and the spatial distribution of the atom beam $X(x)$ and $Z(z)$. The quantity $\theta_{\max}$ is defined [27] as the maximum electron-scattering polar angle that contributes to $I_s(z_D)$. Integration limits of the atom-beam velocity distribution are

$$V_1=\frac{L\sqrt{2mE_0}\left[1-\cos(\theta)\left[\frac{E_k}{E_0}\right]^{1/2}\right]}{M(z_D-z+\Delta z)}\ , \tag{2}$$

$$V_2=\frac{L\sqrt{2mE_0}\left[1-\cos(\theta)\left[\frac{E_k}{E_0}\right]^{1/2}\right]}{M(z_D-z-\Delta z)}\ , \tag{3}$$

where L is defined in Sec. II A, m is the electron mass, E_k is the electron energy after the collision, and M is the atom mass.

The final differential cross section in Ref. [7] is the average of the collision cross sections for two azimuthal angles (θ,ϕ) and $(\theta,\pi-\phi)$, which is one-half of the $\sigma(\theta)$ in Eq. (1) in this paper. To clarify, we will recall arguments from Refs. [7,8] where Bartschat and Madison (BM) analyzed our experimental arrangement.

The following has been stated in Ref. [7]. "The choice of right-hand (σ^+) or left-hand (σ^-) circularly polarized laser light for sodium excitation results[4] in $M_L=+1$ or $M_L=-1$ magnetic sublevels of the $3\,^2P_{3/2}$ prepared atoms, respectively, quantized along the laser propagation axis (natural frame[2]). The scattering intensities of these two states are symmetric with respect to a reflection of the azimuthal scattering angle ϕ about $\phi=\pi/2$, for a given polar scattering angle θ. Consider an atom prepared in the $M_L=+1$ state in the natural frame. In the present experiment the atom detector "sees" at the same time recoiled atoms corresponding to electrons scattered into both (θ,ϕ) and $(\theta,\pi-\phi)$. This means that our measured $\sigma(\theta)$ corresponds to the conditions that 50% of atoms in the interaction region are in the $M_L=+1$ state and 50% are in [the] $M_L=-1$ state, both prepared in the natural frame. Therefore, the same scattering intensity should be observed with both (σ^+) and (σ^-) laser excitation light." In other words, the measured scattering intensity corresponds to the case where 50% of the target atoms are excited to $3\,^2P_{3/2}(F=3, M_F=3)$ and the other 50% to $3\,^2P_{3/2}(F=3, M_F=-3)$ and both $(\theta,\phi=0)$ and $(\theta,\phi=\pi)$ scattering intensities are measured [37]. The magnetic quantum numbers are not observed after the collision.

We recall the comments from Ref. [8] regarding its Eqs. (7) and (8). The natural frame where the quantization axis is perpendicular to the scattering plane has been used in setting up the initial density matrix. Consider the superelastic $3P\rightarrow 3S$ cross section for a completely unpolarized initial ($3P$)Na beam containing an equal amount of atoms in each $M_L=+1,0,-1$ state. As BM state, for any transition between P and S states of different parity, parity conservation of the interaction implies that the scattering amplitudes and, consequently, the cross sections for transitions between the sublevels with magnetic quantum number $M_L=0$ must vanish in this frame. Thus the unpolarized superelastic cross section is given by

$$\sigma_{\rm un}=\tfrac{1}{3}(\sigma_++\sigma_-)=\tfrac{1}{3}(\sigma_{\rm meas})\ , \tag{4}$$

where the factor $\frac{1}{3}$ is introduced to account for the average over the initial orbital angular-momentum components. In the above equation the measured cross section $\sigma_{\rm meas}$ is the same as $\sigma(\theta)$ in Eq. (1). For the cross section $\sigma_{\rm un}$, however, time-reversal invariance of the transition operator (or "detailed balance") may be used. This gives

$$\sigma_{\rm meas}=3\sigma_{\rm un}(3P\rightarrow 3S)=\frac{E_{3S}}{E_{3P}}\sigma_{\rm un}(3S\rightarrow 3P)\ , \tag{5}$$

where E_{3P} and E_{3S} are the projectile energies when the atomic electron is in the $3P$ or the $3S$ state, respectively. In the present case of electron scattering by sodium $E_{3P}=E_{3S}-2.1$ eV.

III. RESULTS AND DISCUSSION

Small-angle superelastic collisions are distinguished by observing the atom deflection in the detector plane caused by electron scattering, since these result in momentum transfer to the atom-beam counter to the initial electron momentum. Thus recoiled-atom intensities $[I_s(z_D)]$ are taken along the same axis as the horizontal atom-beam profiles, opposite the direction of the incoming electron momentum. At each detector position atomic current signals are sampled by the computer, typically every 20 ms. The electron beam is turned on and off at 0.1 Hz by a signal generated by the computer, which acts as a multichannel analyzer with 250 channels each for the electron beam on and the beam off in each scan. There are ten such scans in each run. A typical output of one run is shown in Fig. 6. The signals with the electron beam on (I_{on}) and off (I_{off}) are then averaged separately by the computer. The difference between I_{on} and I_{off} is the measured signal $I_s(z_D)$. A large amount of data is taken at each detector position for each electron energy and averaged to minimize the statistical error. During the data-taking period the laser frequency is monitored by the transmission intensity of the Doppler-free saturation spectrum of the sodium vapor cell to ensure that the laser frequency remains constant. The computer-averaged $I_s(z_D)$ plotted versus detector position (z_D) at 3 and 10 eV are shown in Fig. 7.

The recoil-atom scattering relation [30] between the z coordinate in the detector plane and the electron polar scattering angle θ in the laboratory frame is

$$z = L[\alpha - \beta\cos(\theta)] , \tag{6}$$

where $\alpha = mv/MV$ is the ratio of the electron and the atom momenta before the collision and $\beta = mv_k/MV$ is the ratio after the collision, where $v_k^2 = 2E_k/m$. Since the incident electron propagating in the $+z$ direction gains energy in a superelastic collision, the atom will recoil in the $-z$ direction as long as the electron polar scattering angle is not too large, i.e., $\cos\theta > \alpha/\beta$. Therefore, no atoms other than superelastic scattered atoms can reach the detector. As can be seen from Fig. 7, the scattering

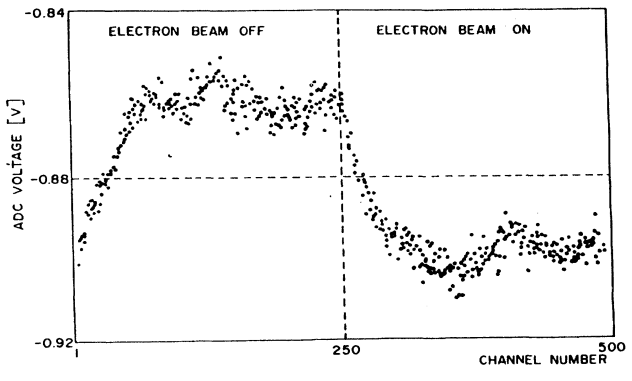

FIG. 6. Typical computer output of one run taken in 100 s for superelastic scattering.

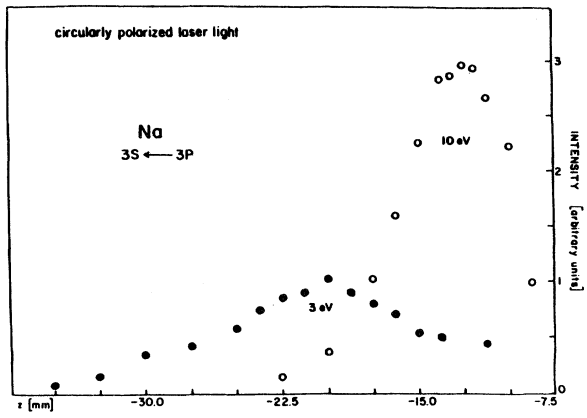

FIG. 7. Computer-averaged superelastic-scattering signal versus detector position. The unscattered atom beam centered at $z = 0$ is off scale on the right. The electron-beam velocity is in the positive z direction.

peak approaches the unscattered atom beam as the electron energy increases. The peak position z_p can be estimated by

$$z_p = (\sqrt{E_0} - \sqrt{E_k})\frac{\sqrt{2m}\,L}{M}\left\langle\frac{1}{V}\right\rangle , \tag{7}$$

where $\langle 1/V\rangle$, the average of the inverse atom beam velocity, is 8.7×10^{-4} s/m in the present case. The largest energy practically realizable in the experiment was 20 eV with the present atom-beam spatial and velocity distributions.

The superelastic scattering experiments on $(3P)$Na have been performed with 3, 5, 10, and 20 eV incident electron energies. The corresponding total collision energies are 5.1, 7.1, 12.1, and 22.1 eV due to an excess of 2.1 eV of the excited sodium above the ground state plus the initial electron energy. These are usually used in calculations.

The measured $I_s(z_D)$ as a function of z_D for each electron impact energy are listed in Table I. The closest detector position to the unscattered atom beam where data are taken at each energy was the position at which the scattering signal was just dominant with respect to the unscattered one. For the $\sigma(\theta)$ determination from $I_s(z_D)$ and other measured parameters, the deconvolution procedure employing Eq. (1) used in the present work and Ref. [7] is essentially the same as that in Ref. [27]. This is a fitting procedure to reproduce measured intensities $I_s(z_D)$ with $\sigma(\theta)$ as the only unknown parameter. An example of the fitted curve and measured intensities for 10 eV is shown in Fig. 8. Differential cross sections $\sigma(\theta)$ thus obtained, in units of 10^{-20} m^2/sr for electron incident energies of 3, 5, 10, and 20 eV, are listed in Table II as σ_{meas}.

We recall that employing the recoil-atom technique, the present experiment is performed with an atom beam polarized in the natural frame, Na$(3P, M_L = +1)$. The corresponding transition is $(3\,^2P_{3/2}, F=3, M_F=3) \rightarrow 3\,^2S_{1/2}$. As explained in Sec. II C, observation with

TABLE I. Computer averaged raw data for electron superelastic scattering by (3P)Na at detector position z_D. Unscattered $I_0(z_D)$ and scattered $I_s(z_D)$ atomic beam intensities in units of $I_0(0)\times 10^{-5}$. Scattered intensities are normalized to an electron beam current 1×10^{-3} A. The excited state fraction $f=0.26$.

z_D (mm)	$I_0(z_D)$	$I_s(z_D)$ 3 eV	5 eV	10 eV	20 eV
−8.9	481.0			2.90	3.71
−10.2	141.0			4.60	4.12
−11.4	86.2	0.57		5.17	3.24
−12.7	60.5	0.79	0.96	5.62	2.40
−14.0	48.3	1.01	1.59	4.87	1.78
−15.2	38.1	1.09	2.01	3.92	1.16
−16.5	30.4	1.43	2.30	2.75	0.90
−17.8	24.5	1.63	2.77	1.95	0.63
−19.1	19.8	1.83	2.47	1.40	0.51
−20.3	16.3	2.08	2.18	0.85	0.39
−21.6	12.0	1.84	1.78		
−22.9	10.7	1.74	1.37		
−24.1	7.8	1.52	1.05		
−25.4	6.6	1.19	0.74		
−26.7	6.0	1.03	0.48		
−27.9	5.3	0.86	0.27		
−29.2	4.8	0.73			
−30.5	4.2	0.61			
−31.8	3.9	0.47			
−33.0	3.6	0.34			
−34.3	3.4	0.26			
−35.6	3.1	0.18			

the employed technique was on $3\,^2P_{3/2}(M_L=\pm 1)\rightarrow 3\,^2S_{1/2}$. The measured $\sigma(\theta)$ is $\sigma_{\text{meas}}=3\sigma_{\text{un}}(3P\rightarrow 3S)$, where $\sigma_{\text{un}}(3P\rightarrow 3S)$ is the cross section for superelastic scattering by unpolarized excited sodium. For practical purposes, we list $\sigma_{\text{un}}(3P\rightarrow 3S)$ in Table II, which is $\frac{1}{3}$ of the measured quantity.

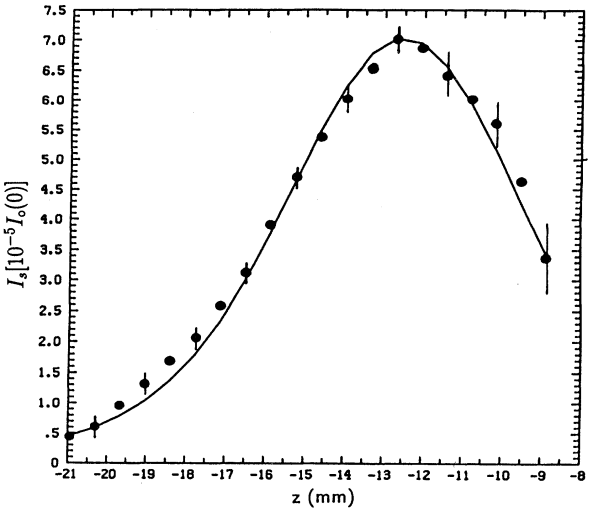

FIG. 8. Fitted curve of (3P)Na superelastic-scattering data at 10 eV electron incident energy: ●, measured scattering intensities; solid line, fitted curve. Error bars denote statistical error. See the text and Ref. [27] for the fitting procedure.

As mentioned in Sec. I, the preliminary result at 3 eV is presented in Fig. 1 of Ref. [7]. These data are $\frac{1}{2}\sigma_{\text{meas}}$ in Table II since the master equation in Ref. [7] contains a factor of $\frac{1}{2}$ on the right-hand side instead of a factor of $\frac{1}{4}$ in the present Eq. (1). An explanation is given in Sec. II C.

The errors in the final results of the differential cross sections are attributable to the systematic and statistical experimental errors, as well as to the uncertainty in the curve-fitting process. The systematic experimental errors include determination of the fraction of excited-state atoms f, ±10%; the atom beam velocity distribution

TABLE II. Differential cross sections $\sigma(\theta)$ for superelastic $(3P\rightarrow 3S)$ electron scattering by sodium atoms in units of 10^{-20} m²/sr. $\sigma_{\text{meas}}=3\sigma_{\text{un}}$, where σ_{meas} is the measured cross section and σ_{un} is the cross section for superelastic $(3P\rightarrow 3S)$ scattering by unpolarized excited sodium atoms. Incident electron energies are indicated. The numbers in brackets denote multiplicative powers of ten.

θ (deg)	3 eV σ_{meas}	3 eV σ_{un}	5 eV σ_{meas}	5 eV σ_{un}	10 eV σ_{meas}	10 eV σ_{un}	20 eV σ_{meas}	20 eV σ_{un}
1	22[1]	73	76[1]	25[1]	16[2]	53[1]	26[2]	87[1]
2	20[1]	67	48[1]	16[1]	11[2]	37[1]	22[2]	73[1]
3	19[1]	63	30[1]	10[1]	72[1]	24[1]	17[2]	57[1]
4	18[1]	60	24[1]	80	54[1]	18[1]	10[2]	33[1]
5	17[1]	56	19[1]	63	42[1]	14[1]	68[1]	23[1]
6	15[1]	50	15[1]	50	36[1]	12[1]	34[1]	11[1]
7	12[1]	40	12[1]	40	30[1]	10[1]	19[1]	63
8	96	32	10[1]	33	26[1]	86	11[1]	37
9	74	25	88	29	24[1]	80	68	23
10	64	21	76	25	20[1]	67	41	14
12	48	16	60	20	15[1]	50		
14	42	14	42	14	10[1]	33		
16	32	11	28	93[−1]	72	24		
18	24	80[−1]	20	67[−1]	36	12		
20	19	63[−1]	17	57[−1]	15	50[−1]		
25	11	37[−1]	10	33[−1]				
30	66[−1]	22[−1]						

$\mathcal{V}(V)$, ±3%; the electron energy distribution $\mathcal{E}(E)$, ±1%; the electron number current i_0, ±2%; the height of the interaction volume h, ±1%; the half-height Δx and half-width Δz, negligible; the detector position z_D, ±3%; and the fluctuation of $I_0(0)$ and $I_0(z_D)$, ±5%. The error in $I_0(z_D)$ actually defines the errors in $X(x)$ and $Z(z)$, while the error in z_D influences the uncertainty in θ and ϕ. All quoted errors are within 1σ of the measured quantity. The statistical errors in the scattering signal $I_s(z_D)$ are ±20%, ±15%, ±7%, and ±5% for 3, 5, 10, and 20 eV, respectively. Adding these errors in quadrature, the total experimental errors are estimated to be ±23%, ±19%, ±14%, and ±13% for 3, 5, 10, and 20 eV electron impact energies, respectively. After propagating the errors through Eq. (1) during the curve-fitting processes, we find that the total errors are about ±50% at all energies. There are fewer experimental points taken at higher energies because of the smaller separation between unscattered and scattered peaks, as explained above. Thus the error due to the evaluation procedure is larger at higher incident electron energies resulting in the same final error attributed to $\sigma(\theta)$ for all energies.

The present results are the only available absolute differential superelastic cross-section measurements, to our knowledge. Also, to our knowledge, there are no absolute inelastic differential cross-section measurements for Na($3S \rightarrow 3P$) at corresponding energies to invoke detailed balancing and compare with the present results. Thus, in Fig. 9 the present data of $\sigma_{un}(3P \rightarrow 3S)$ are compared only with calculations. The incident electron energies are indicated in each plot. Experimental error bars are indicated at selected angles. The full lines are data from Madison, Bartschat, and McEachran [18], calculated with the DWB2 approximation for the $3S \rightarrow 3P$ transition and with detailed balancing converted for comparison with the present results. Results at 3 eV do not have exchange distortion included. The dashed line represents the work of Norcross and co-workers [20,21], calculated using CC at 3 eV (collision energy 5.1 eV). This is the only overlapping energy with the present data since it is the highest energy where the CC is applicable. Finally, the dotted curve represents a calculation by Bray [23] calculated using CCC, appropriate for the full energy range of our experiment. At most of the scattering angles the agreement with calculations is within experimental error, except at over low angles. This latter discrepancy may be attributable to the lower sensitivity of the recoil-atom method in the very low angle region, since the measured intensities depend on $\sigma(\theta)\sin(\theta)$. Large differences between experiment and DWB2 at 3 eV are to be expected since this is too low an energy for the DWB2 approximation to apply.

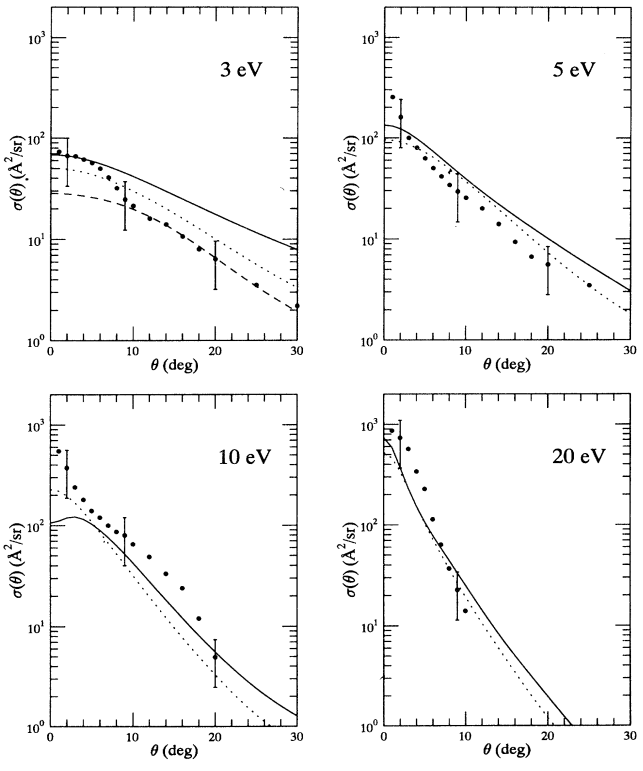

FIG. 9. Differential cross sections for superelastic electron scattering by an unpolarized excited sodium atom $\sigma_{un}(3P \rightarrow 3S)$ in units of 10^{-20} m²/sr. Incident electron energies are indicated. Experimental data: ●, present. Calculated data: full line, Madison, Bartschat, and McEachran [18] (DWB2); dashed line, Norcross and co-workers [20,21] (CC); dotted line, Bray, Fursa, and McCarthy [24] (CCC).

IV. CONCLUSION

In this paper we have presented absolute differential cross sections for superelastic ($3P \rightarrow 3S$) scattering of unpolarized electrons by excited sodium in the energy range 3–20 eV and angular range 1°–30°. Data are shown in Table II and, together with available calculations, in Fig. 9. The initial target state was prepared using laser excitation, so that the atoms were polarized. As discussed, the final result corresponds to an unpolarized initial excited state and detailed balancing for superelastic scattering can be directly invoked to compare the inverse reactions $3S \rightarrow 3P$.

The presented results for superelastic scattering offer a unique experimental approach to the determination of absolute differential cross sections for the scattering by alkali-metal atoms with no calibration involved. Thus we obtain additional insight into the collisional dynamics. Specifically, the polarized recoil-atom scattering results can be related [8] to the corresponding time-reversal experiment with unpolarized atoms, as long as the final state is an S state of even parity and the initial P state has odd parity. This is based on the assumptions [3] that spin-dependent forces, such as the spin-orbit interaction as well as any effect of the nuclear spin, can be neglected in the collision process. As expected, the present experiment reconfirms that these assumptions are acceptable for sodium. Superelastic collisions by laser-excited atoms is the only case where the hyperfine structure can be resolved with present state-of-the-art experimental techniques. Thus, if the equivalent recoil atom $3P \rightarrow 3S$ and $3S \rightarrow 3P$ experiment were performed with heavier alkali metals, it would be an important test of the effects of spin-orbit interactions in heavy-atom collisions.

ACKNOWLEDGMENTS

This work is supported by National Science Foundation Grant No. PHY-9007571. Z.S., C.H.Y., and L.V. acknowledge support by the Physics Department, Old Dominion University during the writing of this paper. We acknowledge the assistance of M. Zuo during the initiation of the experiment.

[1] S. Trajmar and J. C. Nickel, Adv. At. Mol. Phys. **30**, 45 (1992).

[2] N. Andersen, J. W. Gallagher, and I. V. Hertel, Phys. Rep. **165**, 1 (1988).

[3] N. Andersen and K. Bartschat, Comments At. Mol. Phys. **29**, 157 (1993).

[4] J. J. McClelland, M. H. Kelley, and R. J. Celotta, Phys. Rev. A **40**, 2321 (1989).

[5] L. Vušković, M. Zuo, G. F. Shen, B. Stumpf, and B. Bederson, Phys. Rev. A **40**, 133 (1989).

[6] Assume that unpolarized initial states are prepared with an equal population of Na($3P$, $M_L = -1, 0, +1$) magnetic substates. If an unpolarized electron beam crossfires these atoms, one can obtain superelastic differential cross sections by measuring the intensity of scattered electrons that gain 2.1 eV in the collision as a function of θ. These measurements, of course, require knowledge of geometrical parameters, detector efficiency, as well as the densities of both [electron and ($3P$)Na] colliding partners in the interaction region. The results presented in this paper obtained with the recoil atom technique are equivalent to the above measurements.

[7] T. Y. Jaing, M. Zuo, L. Vušković, and B. Bederson, Phys. Rev. Lett. **68**, 915 (1992).

[8] K. Bartschat and D. Madison, Phys. Rev. A **48**, 836 (1993).

[9] I. V. Hertel and W. Stoll, J. Phys. B **7**, 583 (1974).

[10] H. W. Hermann, I. V. Hertel, W. Reiland, A. Stamatović, and W. Stoll, J. Phys. B **10**, 251 (1977).

[11] G. F. Hanne, Cz. Szmytkowski, and M. van der Wiel, J. Phys. B **15**, L109 (1982).

[12] J. J. McClelland, M. H. Kelley, and R. J. Celotta, Phys. Rev. Lett. **55**, 688 (1985).

[13] J. J. McClelland, M. H. Kelley, and R. J. Celotta, Phys. Rev. Lett. **56**, 1362 (1986).

[14] J. J. McClelland, M. H. Kelley, and R. J. Celotta, Phys. Rev. Lett. **58**, 2198 (1987).

[15] J. J. McClelland, M. H. Kelley, and R. J. Celotta, J. Phys. B **20**, L385 (1987).

[16] R. E. Scholten, S. R. Lorentz, J. J. McClelland, M. H. Kelley, and R. J. Celotta, J. Phys. B **24**, L653 (1991).

[17] P. J. O. Teubner and R. E. Scholten, J. Phys. B **25**, L301 (1992).

[18] D. H. Madison, K. Bartschat, and R. P. McEachran, J. Phys. B **25**, 5199 (1992), and private communication.

[19] D. L. Moores and D. W. Norcross, J. Phys. B **5**, 1482 (1972).

[20] H. L. Zhou, D. W. Norcross, and B. L. Whitten, in *Correlations and Polarizations in Electronic and Atomic Collisions and (e,2e) Reactions,* Proceedings of the Sixth International Symposium held at Flinders University, Adelaide, Australia, July 1991, edited by P. J. O. Teubner and E. Weigold, IOP Conf. Proc. No. 122 (Institute of Physics and Physical Society, Bristol, 1992), pp. 39–48, and private communication.

[21] W. K. Trail, M. A. Morrison, H. L. Zhou, B. L. Whitten, K. Bartschat, K. B. MacAdam, T. L. Goforth, and D. W. Norcross, Phys. Rev. A **49**, 3620 (1994).

[22] K. A. Berrington, P. G. Burke, M. Le Dourneuf, W. D. Robb, K. T. Taylor, and Vo Ky Lan, Comput. Phys. Commun. **14**, 367 (1977).

[23] I. Bray, Phys. Rev. A **49**, 1066 (1994).

[24] I. Bray, D. V. Fursa, and I. E. McCarthy, Phys. Rev. A **49**, 2667 (1994), and private communication.

[25] D. H. Madison, K. Bartschat, and R. Srivastava, J. Phys. B **24**, 1839 (1991).

[26] B. Jaduszliwer, P. Weiss, A. Tino, and B. Bederson, Phys. Rev. A **30**, 1255 (1984).

[27] T. Y. Jiang, C. H. Ying, L. Vušković, and B. Bederson, Phys. Rev. A **42**, 3852 (1990).

[28] B. Jaduszliwer, G. F. Shen, and B. Bederson, Phys. Rev. A **33**, 3792 (1986).

[29] G. Wannier, Phys. Rev. **90**, 817 (1953).

[30] M. Zuo, T. Y. Jiang, L. Vušković, and B. Bederson, Phys. Rev. A **41**, 2489 (1990).

[31] B. Jaduszliwer, R. Dang, P. Weiss, and B. Bederson, Phys. Rev. A **21**, 808 (1980).

[32] B. Jaduszliwer, G. F. Shen, J. L. Cai, and B. Bederson, Phys. Rev. A **31**, 1157 (1985).

[33] P. E. Moskowitz, P. L. Gould, S. R. Atlas, and D. E. Pritchard, Phys. Rev. Lett. **51**, 370 (1983).

[34] A. Aspect, J. Dalibard, A. Heideman, C. Salmon, and C. Cohen-Tannoudji, Phys. Rev. Lett. **57**, 1688 (1986).

[35] T. W. Hänsch, I. S. Shahin, and A. L. Schawlow, Phys. Rev. Lett. **27**, 707 (1971).

[36] P. G. Pappas, M. M. Burns, D. D. Hinshelwood, M. S. Feld, and D. E. Murnick, Phys. Rev. **21**, 1955 (1980).

[37] The measured recoiled atom intensity after collsion with an unpolarized electron beam is related to that obtained with electrons if both electrons, scattered to the left as well as to the right, through an angle θ are counted.